Engineering approaches to investigate pneumococcal gene expression regulation and antibiotic resistance development

Sorg, Robin

Chapter 5

Collective Resistance in Microbial Communities by Intracellular Antibiotic Deactivation

This chapter authored by Robin A. Sorg, Leo Lin, G. Sander van Doorn, Moritz Sorg, Joshua Olson, Victor Nizet and Jan-Willem Veening is under revision for *PLoS Biology*.

Abstract The structure and composition of bacterial communities can compromise antibiotic efficacy. For example, the secretion of β-lactamase by individual bacteria provides passive resistance for all residents within a polymicrobial environment. Here, we uncover that collective resistance can also develop via intracellular antibiotic deactivation. Real-time luminescence measurements and single-cell analysis demonstrate that the human pathogen *Streptococcus pneumoniae* grows in medium supplemented with chloramphenicol when resistant bacteria expressing chloramphenicol acetyltransferase (CAT) are present. We show that CAT processes chloramphenicol intracellularly but not extracellularly. In a mouse pneumonia model, more susceptible pneumococci survive chloramphenicol treatment when co-infected with a CAT-expressing strain. Mathematical modeling predicts that stable coexistence is only possible when antibiotic resistance comes at a fitness cost. Strikingly, CAT-expressing pneumococci in mouse lungs were outcompeted by susceptible cells even during chloramphenicol treatment. Our results highlight the importance of the microbial context during infectious disease as a potential complicating factor to antibiotic therapy.

Introduction

Antibiotics are indispensable for fighting bacterial infections. Yet the rapid emergence of resistance during the last decades renders current drugs increasingly ineffective and poses a serious threat to human health[1]. Drug action and bacterial resistance mechanisms are well understood in population assays of isogenic cultures *in vitro*. However, ecological factors and cell physiological parameters in natural environments influence the impact of antibiotics[2,3]. *Streptococcus pneumoniae* (pneumococcus) is an important human pathogen that resides in complex and dynamic host environments. The bacterium primarily populates the nasopharynx of healthy individuals, together with numerous commensal microbiota, and often alongside disease-associated species including *Staphylococcus aureus, Moraxella catarrhalis* and *Haemophilus influenzae*[4–6].

While an individual pneumococcal cell competes for limited resources with all other bacteria present in the niche, it may also benefit from a community setting. In a collective effort, bacteria become recalcitrant to antibiotics when forming biofilms that represent a physical constraint for drug accessibility[7,8]. Additional population-based survival strategies involve the phenotypic diversification of an isogenic population, either to pre-adapt for environmental changes (bet-hedging) or to enable division of labor[9]. Since the impact of most antibiotics is growth rate-dependent[10–12], a bifurcation into growing and non-growing cells increases the drug tolerance for the latter fraction, commonly referred to as persisters[13,14]. Cell-to-cell communication represents another way to react to antibiotic inhibition, by allowing bacteria to coordinate a common response; *S. pneumoniae*, for example, activates the developmental process of competence whereupon it may acquire resistance[15–17]. A quorum-sensing mechanism that compromises antibiotic effectiveness was also found in evolved *Escherichia coli* cultures, where cells of increased resistance induce drug efflux pumps in susceptible cells via the signaling molecule indole[18].

As an alternative to reduced drug susceptibility, bacteria can also clear lethal doses of antibiotics from their environment. High cell densities and thus the presence of many drug target sites may be sufficient to lower the concentration of active compound by titration of free drug molecules[19]. Furthermore, antibiotic degradation via the secretion of β-lactamase enables growth not only of resistant cells but also of susceptible cells in their vicinity[20–22], even across species, as demonstrated for amoxicillin-resistant *H. influenzae* and susceptible *S. pneumoniae*[23,24]. This mechanism is of direct relevance to clinical medicine, and is alternatively referred to as passive or indirect resistance (from the perspective of susceptible cells) or collective resistance (from the perspective of mixed populations)[25].

Here, we describe another mechanism by which bacteria survive antibiotic therapy without obtaining genetic resistance, with the example of the bacteriostatic antibiotic

chloramphenicol (Cm) and the human pathogen *S. pneumoniae*. We show that Cm-resistant pneumococci expressing the resistance factor chloramphenicol acetyltransferase (CAT) can provide passive resistance for Cm-susceptible pneumococci by intracellular antibiotic deactivation. CAT covalently attaches an acetyl group from acetyl-CoA to Cm[26,27] and thus prevents the drug from binding to bacterial ribosomes[28]. Intracellular CAT in resistant bacteria can potently detoxify an entire environment, in growth culture, semisolid surfaces of microscopy slides or in a mouse infection model, supporting the survival and growth of genetically susceptible bacteria in the presence of initially effective Cm concentrations. Our results expand recent findings on the basis of *E. coli* growth cultures and indicate a potential clinical relevance of passive Cm resistance[29,30].

Results

Antibiotic resistance of the pneumococcus

Resistances to all currently prescribed antibiotics have been identified in clinical isolate strains of *S. pneumoniae*[31]. Genes that transfer antibiotic resistance can be classified according to their mode of action[32]. One class keeps the cytoplasmic drug level low by preventing drug entry or by exporting drug molecules. Another class alters the targeted enzymes by modifying their drug binding sites or by replacing the entire functional unit. A third class alters the drug molecules themselves. Only members of the latter group are potential candidates for establishing passive resistance. In the pneumococcus, resistance genes that deactivate antibiotics include aminoglycoside phosphor- or acetyltransferases and CAT. To date, β-lactam antibiotic-degrading enzymes have not been reported in *S. pneumoniae* genomes or plasmids[33].

Standard therapy of pneumococcal infections does not include aminoglycosides because of the relatively high intrinsic resistance of *S. pneumoniae* to members of this antibiotic family. In contrast, Cm, a member of the World Health Organization Model List of Essential Medicines[34], is regularly prescribed throughout low-income countries for infections with *S. pneumoniae* and other Gram-positive pathogens, due to its broad spectrum, oral availability, and excellent tissue distribution including the central nervous system. Recently, the antibiotic was also discussed as candidate for a comeback in developed nations due to spreading resistances against first-line agents[35–37].

To test whether passive resistance emerges from antibiotic-deactivating resistance markers with *S. pneumoniae*, we used the drug-susceptible clinical isolate D39[38]. We constructed an antibiotic-susceptible reporter strain expressing firefly luciferase (*luc*) and antibiotic-resistant strains expressing single-copy genomic integrated kanamycin

3'-phosphotransferase (*aphA1*), gentamicin 3'-acetyltransferase (*aacC1*) and chloramphenicol acetyltransferase (*cat*). Resistant and susceptible cells were grown at a one-to-one ratio and optical density (both strains) and bioluminescence (emitted by susceptible cells only) were measured. Expression of *cat*, but not *aphA1* or *aacCI*, conferred passive resistance to susceptible cells (S1 Fig.), mirroring prior investigations of antibiotic deactivation by resistant isolates of *S. pneumoniae*[39]. Aminoglycosides permeate the bacterial cell only at low frequency[40]; high permeability, however, was recently shown to represents an important precondition for the establishment of passive resistance, explaining why the phenomenon could not be observed with *aphA1* and *aacCI* expression[29].

Collective resistance to chloramphenicol *in vitro*

To characterize the observed Cm collective resistance in more detail, we used the Cm-susceptible strain D-PEP2K1 (from here on Cm^S), which constitutively expresses *luc* and the kanamycin resistance marker *aphA1*[41], and the Cm-resistant strain D-PEP1-pJS5 (from here on Cm^R), which expresses *cat* from plasmid pJS5[42] (see Methods). Luminescence allowed for the real-time estimation of the population size of Cm^S cells, and kanamycin resistance allowed for the monitoring of their viable cell count by plating assays in the presence of kanamycin. Cm represses the growth of susceptible pneumococci at a minimal inhibitory concentration (MIC) of 2.2 μg ml^{-1}, and during Cm exposure, luminescence from *luc* expression of susceptible pneumococci was previously shown to decrease at a rate that depends on the applied Cm concentration[12]. This observation was confirmed by Cm^S exposure to 3 μg ml^{-1} and 5 μg ml^{-1} Cm (Fig. 1a). However, when Cm^S was co-inoculated with CAT-expressing Cm^R, luciferase expression (indicative for growth of the Cm^S cell fraction) recovered, even though the medium initially contained Cm concentrations of more than two times the MIC (Fig. 1a). Luminescence recovery in mixed population assays (Cm^R + Cm^S) exceeded the values measured with Cm^S monoculture by up to 10–fold, and plating assays (with kanamycin) revealed that the difference in viable cell count was 1000–fold greater after 8 h of co-cultivation (Fig. 1a, b). Although Cm is commonly regarded as bacteriostatic, bactericidal activity has also been demonstrated against *S. pneumoniae*[43], explaining the observed decrease in viability of Cm^S monoculture (Fig. 1b).

To confirm that Cm^R cells actually deactivate Cm in the growth medium, we analyzed culture supernatant by high-performance liquid chromatography (HPLC)[44]. As shown in Figure 1c, within 4 h of growth, Cm^R cells entirely converted an initial Cm concentration of 5 μg ml^{-1}, as evidenced by the disappearance of the corresponding Cm peak at wavelength 278 nm. New peaks (at later elution times) appeared and gradually increased in HPLC profiles of culture supernatants collected after 1, 2 and 4 h of cultivation; these peaks

were previously shown to correspond to acetylated Cm derivates (1- and 3-acetylchloramphenicol)[44].

Next, we focused on whether the initial amount of CAT-expressing Cm^R cells was important for the survival and growth of Cm^S cells during drug treatment. To test this, we inoculated microtiter plate wells with a fixed number of Cm^S cells (OD 0.001, corresponding to ~ 1.5×10^6 CFUs ml^{-1}) while varying the number of Cm^R cells (Fig. 1d). High inoculation densities of Cm^R cells (OD 0.01) resulted in a fast recovery of luminescence activity of Cm^S cells; however, the peak of luminescence was lower compared to intermediate Cm^R inoculation densities. This difference can be explained by cells reaching the carrying capacity of the growth medium before the pool of Cm is completely deactivated; luciferase expression activity was previously shown to slow down when cultures reach high cell densities (above ~ OD 0.05)[41]. Relatively low Cm^R inoculation densities (OD 0.0001) also limited luminescence recovery of Cm^S cells during co-cultivation. This finding likely reflects fewer Cm^R cells requiring more time to deactivate Cm, resulting in increased time spans of Cm^S drug exposure. Prolonged drug exposure of susceptible pneumococci was previously shown to result in increasing lag periods after drug removal, indicating a more severe perturbation of cell homeostasis[12]. The time span before outgrowth of Cm^S cells consequently consists of both the period required for drug clearance (by Cm^R cells) and the period required to re-establish intracellular conditions allowing for cell-division.

Intracellular deactivation of chloramphenicol

To test whether Cm processing by CAT is an intracellular process, or if it takes place after secretion or cell lysis, we examined the potential of the culture supernatant and the cytosolic content of Cm^R cells to deactivate Cm (assay scheme in Fig. 1f). Pre-cultured Cm^R cells were diluted to OD 0.02 and translation activity was blocked by adding 1 μg ml^{-1} tetracycline (Tc; *S. pneumoniae* D39 MIC: 0.26 μg ml^{-1})[12] for 1 h at 37°C to prevent ongoing protein synthesis and thus CAT expression. Next, the Tc-treated culture was split into three fractions: cell pellet (P) and culture supernatant (S), separated via centrifugation, and cell culture lysate (L), obtained by sonication. The cell pellet was re-suspended in C+Y medium containing 3 μg ml^{-1} Cm (and 1 μg ml^{-1} Tc), and 3 μg ml^{-1} Cm was added to the culture supernatant and the lysate, followed by incubation at 37°C. After 2 h, the remaining cells and cell debris were removed by centrifugation and filtration, and the treated medium was used to test cell growth of a Tc-resistant variant of the Cm^S strain. Neither the culture supernatant (S) nor the lysate (L) could support growth of Cm^S, while medium pre-incubated with the cell pellet (P) did (Fig. 1e). Together, these experiments indicate that CAT is only active inside living cells, where acetyl-CoA is present[26,27].

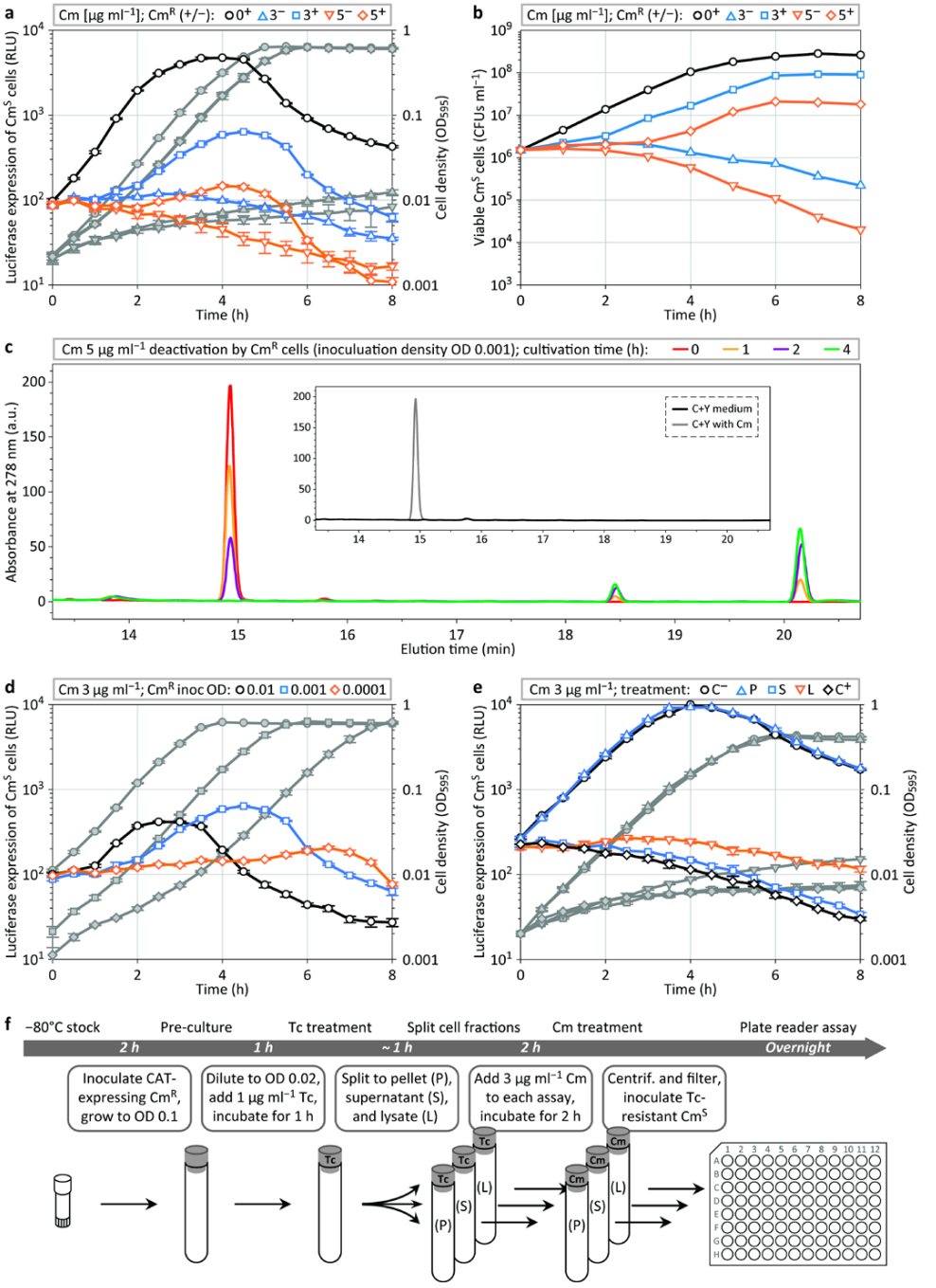

Figure 1 | Chloramphenicol deactivation during mixed population assays. (**a**) Plate reader assay sets in quadruplicate (average and s.e.m.) measuring luciferase expression (symbols with color outline) and cell density (corresponding grey symbols) of

chloramphenicol-susceptible *S. pneumoniae* D-PEP2K1 (Cm^S) growing in the presence of 0, 3 and 5 µg ml^{-1} chloramphenicol (Cm), respectively, in presence (+) or absence (−) of resistant D-PEP1-pJS5 (Cm^R) cells. (**b**) Development of the count of viable Cm^S cells (CFUs ml^{-1}, colony-forming units per ml) during the cultivation assay presented in **a**, determined via plating in the presence of kanamycin; average values of duplicates are shown. (**c**) Culture supernatant samples after 0, 1, 2 and 4 h of Cm^R cultivation (inoculation density OD 0.001) in the presence of 5 µg ml^{-1} Cm, analyzed for Cm content by HPLC separation and UV detection at 278 nm. (**d**) Luciferase expression and cell density profiles of Cm^S cells treated with 3 µg ml^{-1} chloramphenicol (inoculation density OD 0.001) in dependency of the inoculum size of Cm^R cells. (**e**, **f**) Cm^S luciferase expression and growth analysis (**e**) in chloramphenicol-supplemented medium (3 µg ml^{-1}) that was pretreated with Cm^R cell pellet (P), culture supernatant (S) and culture lysate (L), and controls without (C^-) and with chloramphenicol (C^+); schematic overview of the assay (**f**) (see also Methods).

Single-cell observations of collective resistance

Since the above-mentioned experiments were performed in bulk assays, we wondered whether CAT-expressing bacteria would also efficiently deactivate Cm, and thus support the growth of susceptible cells, in a more complex environment, such as on semi-solid surfaces. To do so, we spotted Cm^R cells together with Cm-susceptible D-PEP33 cells expressing GFP on a matrix of 10% polyacrylamide C+Y medium containing 3 µg ml^{-1} Cm. Indeed Cm-susceptible D-PEP33 cells were able to grow and divide under these conditions (S2 Fig.).

S. pneumoniae cohabitates the human nasopharynx with other bacteria, such as *S. aureus* [6]. Therefore, we investigated whether CAT-expressing *S. aureus* could also support growth of Cm-susceptible *S. pneumoniae* in environments containing Cm. As shown in Figure 2, all *S. aureus* cells grew and divided from the starting point of the experiment, while *S. pneumoniae* Cm^S cells did not grow initially. However, after 8 h, a fraction of Cm^S cells grew out to form microcolonies. Note that Cm^S cells spotted in the absence of *S. aureus* did not grow under these conditions.

Requirements for stable coexistence

The observation that Cm^S cells grow only when Cm-deactivating cells are present in their close vicinity (Fig. 2) suggests that the establishment of collective resistance requires Cm^S and Cm^R bacteria to be present in the same niche. However, such coexistence is subject to ecological constraints (e.g., the competitive exclusion principle)[45], particularly if susceptible and resistant strains compete for the same limiting resource. We therefore developed an ecological model to assess the scope for coexistence between CAT-producing bacteria and an antibiotic-susceptible strain (S1 Text). Consistent with this objective, we employed a

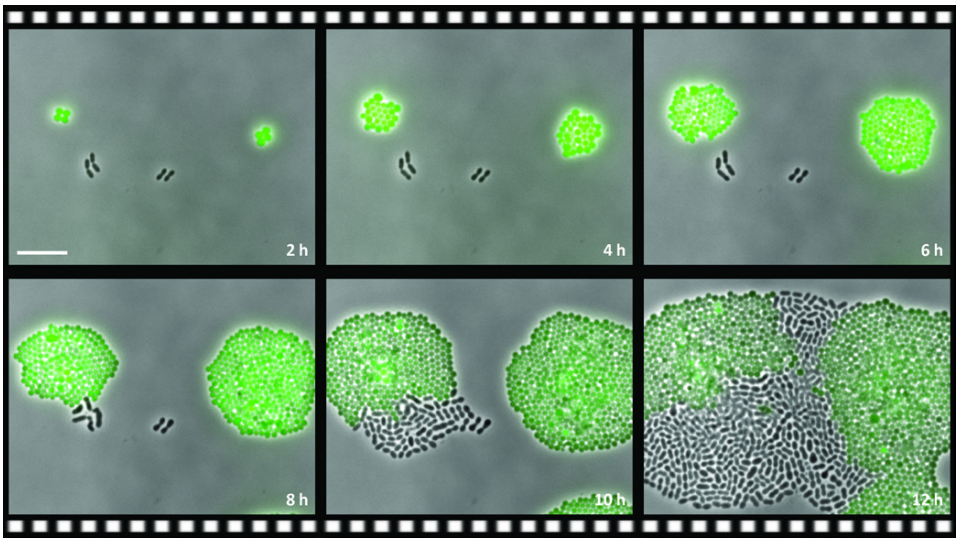

Figure 2 | Interspecies collective resistance. Still images (overlay of phase contrast and fluorescence microscopy) of a time-lapse experiment of *S. pneumoniae* D-PEP2K1 (Cm^S), co-cultivated with a strain of the pneumococcal niche competitor *Staphylococcus aureus* (strain LAC pCM29) that expresses CAT and GFP, growing on a semi-solid surface supplemented with 3 µg ml^{-1} chloramphenicol. Scale bar, 10 µm.

minimalist modeling strategy and characterized all possible outcomes of the interaction between Cm^S and Cm^R bacteria, rather than aiming for a precise quantitative reconstruction of the experimental conditions. In fact, the model considers a worst-case scenario for coexistence: the two populations grow in a well-mixed, homogeneous environment and are limited by the same resource. Nonetheless, we found that coexistence between Cm^R and Cm^S bacteria was feasible (Fig. 3a, b), be it under a restricted range of conditions (Fig. 3c and S3 Fig.). A mathematical analysis of the model (S1 Text) indicates that resistant and susceptible bacteria can establish a stable coexistence when CAT expression has a modest fitness cost. Without such a cost, the Cm^R strain is predicted to outcompete the Cm^S strain in the presence of antibiotics. Conversely, if the cost of expressing resistance is too high, the Cm^S strain will be the superior competitor. Interestingly, the model furthermore predicts parameter ranges that result in the extinction of mixed populations during drug treatment, while Cm^R populations on their own could survive (S3 Fig. and S4 Fig.). A second condition for coexistence demands that the Cm^R population has a significant impact on the extracellular Cm concentration in its ecological niche. This requires that the population

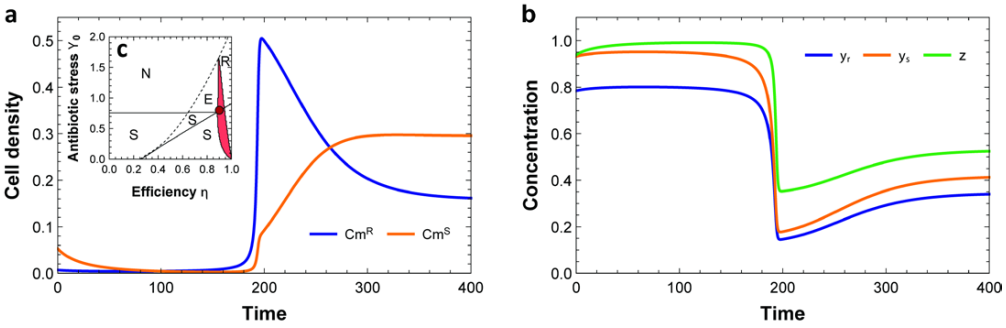

Figure 3 | Population dynamics of bacterial communities. (**a**) Simulated growth trajectories for chloramphenicol-resistant (Cm^R) and chloramphenicol-susceptible (Cm^S) populations subject to antibiotic stress and resource competition. (**b**) Dynamic of intracellular Cm (y_r and y_s) and growth-limiting resource (z). Simulation time is scaled relative to the mean residence time of cells in a chemostat, which is equal to the generation time at steady state. At low population densities, the Cm^R strain can grow, whereas Cm^S cannot, due to a high concentration of Cm. However, the invasion of Cm^R lowers antibiotic stress, generating permissive conditions for the growth of Cm^S cells. The chemostat is then rapidly colonized by both strains (shortly after $t = 180$), until the resource becomes limiting. From that moment onwards, total cell density changes little, while the relative frequencies of the two strains continue to shift. Eventually, a stable equilibrium is reached, at which the cost and benefit of CAT expression (i.e., reduced growth rate efficiency for Cm^R cells versus their lower intracellular Cm concentration) balance out. Inset (**c**) Coexistence, as observed in **a**, is possible for a restricted range of parameters (highlighted in red; the dark-red dot pinpoints the arbitrary parameter set used in the simulation shown in **a** and **b**: $r = 20.0$, $\eta = 0.9$, $k_z = 4.0$, $c = 1.0$, $p = 50.0$, $h_Y = 0.25/Y_0$, $k_Y = 2.5/Y_0$, $d = 30.0/Y_0$ and $Y_0 = 0.8$). Alternative model outcomes, which were identified by a numerical bifurcation analysis (see S1 Text and S3 Fig.), include: establishment of Cm^S only (area S), establishment of Cm^R only (area R), no bacterial growth (area N) and competition-induced extinction (area E, where Cm^S bacteria first outcompete Cm^R bacteria, and subsequently are cleared by the antibiotic; see S4 Fig.).

density reached at steady state must be high, so that coexistence can be stabilized by frequency-dependent selection, generated by a negative feedback loop between the relative abundance of drug-deactivating cells and the level of antibiotic stress in the environment.

We note that competitive exclusion acts at a local scale in structured environments, where the presence of spatial gradients in Cm and resources may help to create refuges in which either strain can escape competition from the other. In addition, we expect that coexistence between resistant and susceptible bacteria would be promoted *in vivo* by previously evolved ecological niche partitioning between co-occurring species.

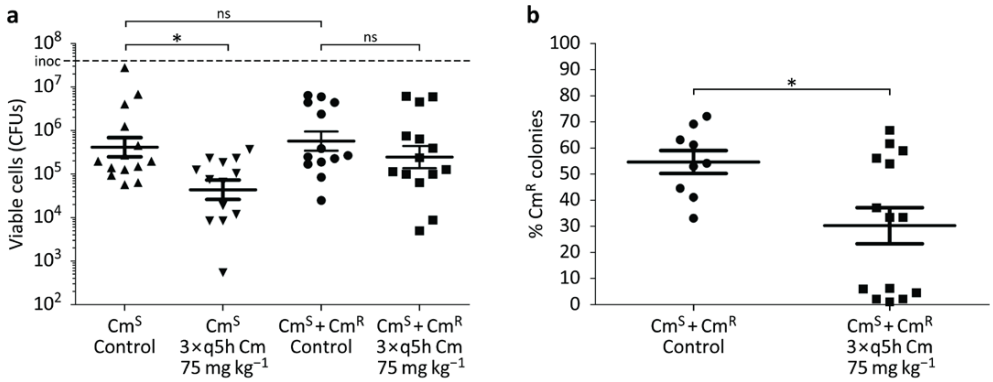

Figure 4 | Cross-protection in a mouse pneumonia model. (**a**) 8 week old female CD1 mice were infected intratracheally with Cm^S pneumococci or an equivalent amount of Cm^S+Cm^R pneumococci in a one-to-one ratio. 1 h post infection mice were treated with one intraperitoneal injection of Cm 75 mg kg^{-1}, followed by two additional doses spaced 5 h apart. Control mice received an injection of the vehicle alone; n = 14 for Cm^S control; 13 for Cm^S Cm-treated; 13 for Cm^S+Cm^R control; and 14 for Cm^S+Cm^R Cm-treated. Data plotted as average and s.e.m. of two independent experiments combined. Dashed line 'inoc' denotes the initial inoculum. **P < 0.05*; one-way ANOVA with Tukey's multiple comparison post-test. (**b**) Bacterial colonies recovered from the Cm^S+Cm^R control and Cm^S+Cm^R Cm-treated mice were individually picked and used to inoculate THY media in 96-well plates. These 96-well plates were then used to inoculate 96-well plates with THY media containing either 15 µg ml^{-1} Cm or 100 µg ml^{-1} kanamycin to determine whether or not the original bacterial colony was Cm^S or Cm^R; n = 9 for Cm^S+Cm^R control and 14 for Cm^S+Cm^R Cm-treated. Data plotted as average and s.e.m. of two independent experiments combined. **P* = 0.04; Mann-Whitney U-test.

In vivo collective chloramphenicol resistance

A general prediction from our mathematical model (S1 Text) is that coexistence of Cm^S and Cm^R in the presence of the antibiotic is precluded when the production of CAT carries no fitness cost; we expect this prediction to apply likewise in more complex environments with spatial and/or temporal heterogeneity in Cm concentrations. However, *in vitro*, in short-term experiments, we did not observe any obvious fitness cost for CAT expression (such as reduced growth rates or a reduced maximum cell density) (Fig. 1). Nevertheless, *in vivo*, a fitness cost might come into existence because resistant cells that grow rapidly might be preferentially targeted by the host innate immune system, as previously shown for commensal and pathogenic bacteria including *E. coli* and *S. aureus*[46]. We tested the activity of the human antimicrobial peptide LL-37 in dependency of Cm treatment, and found indeed increased killing efficiency against CAT-expressing *S. pneumoniae* (S5 Fig.). Furthermore, while collective resistance could be successfully demonstrated *in vitro*, the

phenomenon might not occur in more complex environments *in vivo*, such as in an animal infection model, because of a different flux balance between local Cm deactivation and restoration of effective drug concentrations via diffusion from surrounding tissues. To examine whether a coexistence between Cm^S and Cm^R is possible under therapy *in vivo*, we performed intratracheal infection of 8 week old female CD-1 mice with Cm^S alone and the combination of Cm^S+Cm^R.

In the absence of Cm treatment, we observed no significant difference in the amount of viable bacteria recovered from the lungs 24 h after infection with Cm^S alone versus Cm^S+Cm^R at a one-to-one ratio (Fig. 4a). When mice were given three doses of 75 mg kg^{-1} Cm once every 5 h, mice infected with Cm^S alone demonstrated a significant drop of 1 log–fold versus the untreated control. This is in contrast to mice co-infected with Cm^S+Cm^R, where Cm treatment did not significantly reduce the number of viable bacteria recovered from the lung versus the untreated control (Fig. 4a). In the one-to-one mixed infection, approximately equal numbers of Cm^S and Cm^R cells were recovered in the absence of Cm treatment, 46% Cm^S and 54% Cm^R (Fig. 4b). Surprisingly, with Cm treatment, 6 out of 14 animals had a dramatic increase in the percentage of Cm^S cells versus Cm^R cells. No pneumococcal colonies recovered could grow in both Cm and kanamycin containing media, excluding the possibility that horizontal gene transfer of the *cat* gene occurred during co-infection. Together, these results show that passive Cm resistance and the coexistence of resistant and susceptible cells also occurs *in vivo*, associated with a fitness cost to the Cm^R niche members benefiting the Cm^S subpopulation.

Discussion

This work elucidates that CAT, which is commonly found as a resistance marker in the human microbiome[47–49], can effectively protect Cm-susceptible pneumococci from the activity of the drug within local environments occupied by CAT-expressing cells. Because of its potency, long shelf live, and low cost, chloramphenicol remains a mainstay of broad-spectrum antibiotic therapy in several countries in Africa, the Indian subcontinent and China[50]. The rise of multidrug resistance among human pathogens has also provoked interest in re-evaluating Cm for certain serious infections in developed countries[35–37]. This work points out some caveats in using Cm to target human pathogens on mucosal surfaces since CAT-expressing commensals might provide passive resistance.

CAT can only deactivate Cm inside living cells (Fig. 1e, f), presumably because it needs acetyl-CoA to acetylate and deactivate the target drug[26,27]. We show that Cm deactivation and collective resistance via CAT is not limited to *S. pneumoniae*, since CAT-expressing *S. aureus* can also support the local growth of pneumococci in the presence of

initially effective Cm concentrations (Fig. 2). Collective resistance by CAT does not only occur *in vitro* but also *in vivo* in a mouse pneumonia model (Fig. 4). Strikingly, when Cm-treated mice were co-infected with CAT-expressing and Cm-susceptible pneumococci, the susceptible bacteria outcompeted the resistant ones (Fig. 4). We previously showed that the susceptibility of bacteria towards antimicrobial peptides, produced by the host innate immune system, is markedly diminished in the presence of bacteriostatic antibiotics; Cm-inhibited *E. coli*, for example, are less efficiently cleared by the human peptide LL-37[46]. We could demonstrate that this mechanism also takes place in *S. pneumoniae* (S5 Fig.). When Cm was added to LL-37 treatment of pneumococci, the number of Cm^S cells recovered was 1 log–fold higher compared with Cm^R cells (S5 Fig.). As shown before, this effect occurs because bacteriostatic antibiotic, such as Cm, inhibit the growth of susceptible bacteria, and thereby reduce the susceptibility to host antimicrobial peptides that target bacterial division; Cm-resistant bacteria, in contrast, maintain fast growth in the presence of Cm and are therefore more rapidly killed by host antimicrobial peptides *in vivo*[46]. This phenomenon may therefore represent a contributing factor underlying our findings of the mouse pneumonia model. In this framework, rapidly growing Cm^R cells would suffer immune clearance, while the initially non-growing Cm^S are less efficiently targeted by host defense factors. Once the Cm concentration has dropped sufficiently, Cm^S cells can outgrow and outcompete the diminished Cm^R population.

Our work with CAT and pneumococcus extends the known phenomenon of passive resistance via secretion of β-lactamase, and on recent findings of collective resistance of bacterial communities[29,30]. This mechanism could also appear with other antibiotic degrading resistance factors in other bacteria[29], and may even emerge for synthetic antibiotic compounds[51]. In light of numerous reports of prevalence of drug resistance in pathogens, successful antibiotic therapy might become increasingly complicated with the occurrence of collective resistance. The phenomena may furthermore give rise to multidrug resistance of bacterial communities, in which individual resistances are crowdsourced to different bacterial community residents[2,18,30]. Our mathematical model, however, predicts that such crowdsourcing is only sustainable when resistance expression comes at a (modest) fitness cost (S3 Fig.), and competitive exclusion is avoided by strong ecological feedback or alternative mechanisms (such as spatiotemporal structure or previously evolved niche partitioning). Nevertheless, even if coexistence is limited, the prolonged survival of susceptible cells within resistant communities may already represent an issue, by increasing the opportunity for horizontal gene transfer during antibiotic selection pressure. Passive resistance might consequently represent an important factor towards the development of genetic multidrug resistance.

Methods

Strains and growth conditions

S. pneumoniae D-PEP2K1 (Cm^S), a chloramphenicol-susceptible D39 derivate strain that constitutively expresses firefly luciferase and a kanamycin resistance marker was used throughout. The Tc-resistant variant of this strain contained the Tc resistance gene *tetM* integrated at the *bgaA* locus, obtained via transformation with pPP1[52]. Firefly luciferase has a reported half-life of 3 min in *S. pneumoniae*, and luminescence therefore gives real-time information on the level of gene expression activity[41,53]. *S. pneumoniae* D-PEP1-pJS5 (Cm^R), expressing CAT from plasmid pJS5 was used as standard for a chloramphenicol-resistant strain. Initial experiments were carried out with the Cm-resistant strain D-PEP1C3 that expresses CAT from a strong synthetic promoter. *S. pneumoniae* D-PEP33 expressing GFP was used as a Cm-susceptible strain in time-lapse microscopy experiments[41]. *S. aureus* experiments were performed with strain LAC pCM29 [54] that constitutively expresses CAT and GFP.

S. pneumoniae and *S. aureus* cells were grown in C+Y medium (pH 6.8), supplemented with 0.5 μg ml^{-1} D-luciferin for luminescence measurements, at 37°C[55]. Pre-cultures for all experiments were obtained by a standardized protocol, in which previously exponentially growing cells from −80°C stocks were diluted to OD (600 nm, path length 10 mm) 0.005 and grown until OD 0.1 in a volume of 2 ml medium inside tubes that allow for direct in-tube OD measurements. To determine the number of colony-forming units, *S. pneumoniae* cells were plated inside Columbia agar supplemented with 3% (v v^{-1}) sheep blood and incubated overnight at 37°C.

Microtiter plate reader assays

Costar 96-well plates (white, clear bottom) with a total assay volume of 300 μl per well were inoculated to the designated starting OD value. Microtiter plate reader experiments were performed using a TECAN infinite pro 200 plate reader (Tecan Group) by measuring every 10 min with the following protocol: 5 s shaking, OD (595 nm, path length 10 mm) measurement with 25 flashes, luminescence measurement with an integration time of 1 s.

In mixed population assays (shown in Fig. 1a) all cultures were inoculated with Cm^S cells to an initial cell density of OD 0.001. Cm^R cells were inoculated to the same density, and control cultures without Cm^R cells contained equal amounts of Cm-sensitive D39 wild type cells to correct for unspecific effects such as drug-titration via cellular Cm binding.

HPLC analysis

Culture supernatants were obtained by Cm^R cultivation (inoculation density OD 0.001) in the presence of 5 μg ml^{-1} Cm in microtiter plates (as described above). Four wells were sampled and pooled per time point (combined volume of 1.2 ml), centrifuged to remove cells and filtered through a 0.2 μm filter. HPLC analysis was carried out using an Agilent 1260 Infinity system (Agilent Technologies) with UV detection at 278 nm (maximum absorbance of Cm)[44]. An Aeris Peptide XB-C18 column (Phenomenex) with 3.6 μm particle and a size of 250 × 4.60 mm was used. Reversed-phase chromatography was carried out at a constant flow rate of 1 ml min^{-1}, with the mobile phase consisting of solution A: 10 mM sodium acetate buffer (pH 6.0) containing 5% acetonitrile (v v^{-1}) and solution B: acetonitrile 0.1% TFA, according to the following protocol: 100 μl sample loading, 3 min 10% B, 20 min gradient 10% to 50% B, 1 min gradient 50% to 95% B, 3 min 95% B, 1 min gradient 95% to 10% B, 6 min 10% B.

Microscopy

A Nikon Ti-E microscope equipped with a CoolsnapHQ2 camera and an Intensilight light source was used. Time-lapse microscopy was carried out by spotting pre-cultured cells on 10% polyacrylamide slides inside a Gene Frame (Thermo Fisher Scientific) that was sealed with the cover glass to guaranty stable conditions during microscopy. The polyacrylamide slide was prepared with growth medium containing 3 μg ml^{-1} Cm. Images of fluorescing cells were taken with the following protocol and filter settings: 0.3 s exposure for phase contrast, 0.5 s exposure for fluorescence at 440–490 nm excitation via a dichroic mirror of 495 nm and an emission filter of 500–505 nm. Temperature during microscopy was controlled by an Okolab climate incubator, and images were taken every 10 min during 20 h at 37°C.

Mouse infection model

The murine pneumonia model was performed with slight modifications as previously described[56]. Based on pilot experiments, we estimated that the number of animals required to observe a statistical difference between the groups would exceed the technical limit of animals that could be inoculated and treated per day. Therefore, the experiment was split into two days with the original pool of animals randomized to each group at the start of the multi-day experiment. Prior to statistical analysis, the data was combined. Note that all intratracheal infections were performed in a blinded fashion with respect to Cm or vehicle

treatment. 8 week old female CD1 mice (Charles River Laboratories) with an average body weight of 28 g were used. Fresh cultures of Cm^S and Cm^R were started in 10 ml of Todd-Hewitt broth containing 2% yeast extract (THY) and 10 ml of THY supplemented with 5 μg ml^{-1} Cm respectively. Cultures were grown at 37°C in a 5% CO_2 incubator until OD (600nm) 0.6. Bacteria were washed twice with PBS via centrifugation at 3220×g at room temperature and concentrated in PBS to yield 3.5×10^7 CFU in the inoculation volume of 40 μl. For mixed infections, an equal volume of concentrated Cm^S and Cm^R pneumococci were combined. Mice were anesthetized with 100 mg kg^{-1} ketamine and 10 mg kg^{-1} xylazine. Once sedated, the vocal chords were visualized using an operating otoscope (Welch Allyn) and 40 μl of bacteria was instilled into the trachea during inspiration using a plastic gel loading pipette tip. Mice were placed on a warmed pad for recovery. After 1 h, one intraperitoneal injection of Cm 75 mg kg^{-1} or vehicle controls was given, followed by two additional doses spaced 5 h apart. Mice were sacrificed with CO_2 24 h after infection.

To enumerate total surviving bacteria in the lungs, both lung lobes were removed and placed in a 2 ml sterile micro tube (Sarstedt) containing 1 ml of PBS and 1 mm silica beads (Biospec). Lungs were homogenized by shaking twice at 6000 rpm for 1 min using a MagNA Lyser (Roche), with the specimens placed on ice as soon as they were harvested. Aliquots from each tube were serially diluted for CFU enumeration on THY plates. To determine whether or not a colony was Cm^S or Cm^R, individual colonies from the THY plates were picked and transferred into 100 μl of THY media in 96-well plates. 96-well plates were incubated overnight at 37°C in a 5% CO_2 incubator. After overnight incubation, wells were mixed, and 5 μl of media from each well was transferred into 100 μl of THY containing 15 μg ml^{-1} Cm or 100 μg ml^{-1} kanamycin. 96-well plates were once again incubated overnight at 37°C in a 5% CO_2 incubator, and wells were finally assessed for the presence or absence of a bacterial cell pellet. Chloramphenicol (≥98% purity; Sigma) for animal injection was prepared as follows: 40 mg ml^{-1} of Cm was dissolved in 800 μl of 70% ethanol in PBS to make a 50 mg ml^{-1} stock solution. This stock solution was diluted in PBS to 3.75 mg ml^{-1} for intraperitoneal injection into mice at 75 mg kg^{-1}. All animal studies were performed under protocols approved by the UCSD Institutional Animal Use and Care Committee.

Modeling

The model describes the dynamic of a co-culture of CAT-expressing (Cm^R) and Cm-susceptible (Cm^S) bacterial cells, growing in the presence of Cm in a chemostat environment. The two strains, with population densities x_r and x_s, respectively, compete for

a growth limiting resource, z. Cm is assumed to inhibit growth; we separately keep track of the intracellular concentrations of Cm (y_s in susceptible cells and y_r in resistant cells) and its concentration in the extracellular medium y_m. The equations for the growth of the two bacterial populations and the growth-limiting resource are given by:

$$\begin{aligned} \frac{dx_s}{d\tau} &= r\frac{z}{k_z+z}\frac{h_y}{h_y+y_s}x_s - x_s, \\ \frac{dx_r}{d\tau} &= \eta r\frac{z}{k_z+z}\frac{h_y}{h_y+y_r}x_r - x_r, \\ \frac{dz}{d\tau} &= (1-z) - cr\frac{z}{k_z+z}\left(x_s\frac{h_y}{h_y+y_s} - x_r\frac{h_y}{h_y+y_r}\right), \end{aligned} \quad [1]$$

where r is the maximum growth rate of Cm^S cells, η is the relative growth efficiency of Cm^R cells, c is the resource consumption rate, and k_z and h_y, respectively, are the half-saturation and inhibitory constants of the growth function. Time, resource concentration and cell densities have been scaled relative to the flow rate of the chemostat, the resource concentration in the inflow medium, and the number of cells that fit in the chemostat volume, respectively, in order to reduce the number of free parameters (see S1 Text for details).

The concentrations of Cm in the different compartments, which have been scaled relative to the Cm concentration in the inflow medium, change according to the equations:

$$\begin{aligned} \frac{dy_m}{d\tau} &= \frac{1}{1-x_s-x_r} - p\frac{x_s(y_m-y_s)+x_r(y_m-y_r)}{1-x_s-x_r} - y_m - y_m\frac{d\ln(1-x_s-x_r)}{d\tau}, \\ \frac{dy_s}{d\tau} &= p(y_m-y_s) - y_s - y_s\frac{d\ln x_s}{d\tau}, \\ \frac{dy_r}{d\tau} &= p(y_m-y_r) - d\frac{y_r}{k_y+y_r} - y_r - y_r\frac{d\ln x_r}{d\tau}. \end{aligned} \quad [2]$$

The processes described by the terms on the right-hand side include inflow of Cm into the medium, passive transport of Cm between compartments at rate p, outflow from the chemostat, degradation of Cm by CAT in Cm^R cells (according to Michaelis-Menten kinetics with maximum rate d and half-saturation constant k_y), and concentration changes due to fluctuations in the volume of the compartments. Equations [1] and [2] were solved numerically using *Mathematica* (Wolfram) or simulation software written in C^{++} (used for the numerical bifurcation analysis; based on a Runge-Kutta integration algorithm with adaptive step-size control).

Supplementary Text

S1 Text. Derivation of the mathematical model and model analysis.

S1.1. Model specification. We model a co-culture of genetically resistant (CAT-expressing; Cm^R) and genetically susceptible (Cm^S) bacterial cells, growing in the presence of chloramphenicol (Cm) in a chemostat environment. The two strains, which are assumed to be identical except for aspects directly associated with CAT expression, compete for a common limiting resource. The concentration of the resource, Z, changes through time according to the differential equation:

$$\frac{dZ}{dt} = \frac{Q}{V_{\text{tot}}}(Z_0 - Z) - \frac{N_{\text{s}}}{V_{\text{tot}}}\text{C}(Z, Y_{\text{s}}) - \frac{N_{\text{r}}}{V_{\text{tot}}}\text{C}(Z, Y_{\text{r}}) \qquad [3]$$

where Q is the flow rate of the chemostat, V_{tot} is its total volume, Z_0 is the concentration of the resource in the inflow medium, N_{s} and N_{r} denote the number of susceptible and resistant cells in the chemostat, and C is the per-capita resource-consumption rate, which is a function of the resource concentration and the intracellular concentrations of Cm in susceptible and resistant cells, Y_{s} and Y_{r}, respectively (see equation [6] below). The antibiotic also occurs in the medium, where its concentration is given by Y_{m}.

The following equations describe the change of the number of antibiotic molecules within cells and in the medium, due to inflow and outflow of the chemostat (of medium and cells), passive diffusion of Cm between medium and cell compartments, and degradation of the antibiotic in Cm^R cells:

$$\begin{aligned}
\frac{d(V_{\text{m}}\,Y_{\text{m}})}{dt} &= Q\left(Y_0 - \frac{V_{\text{m}}}{V_{\text{tot}}}Y_{\text{m}}\right) - PN_{\text{s}}(Y_{\text{m}} - Y_{\text{s}}) - PN_{\text{r}}(Y_{\text{m}} - Y_{\text{r}}) \\
\frac{d(vN_{\text{s}}\,Y_{\text{s}})}{dt} &= PN_{\text{s}}(Y_{\text{m}} - Y_{\text{s}}) - \frac{Q}{V_{\text{tot}}}vN_{\text{s}}\,Y_{\text{s}} \\
\frac{d(vN_{\text{r}}\,Y_{\text{r}})}{dt} &= PN_{\text{r}}(Y_{\text{m}} - Y_{\text{r}}) - N_{\text{r}}\text{D}(Y_{\text{r}}) - \frac{Q}{V_{\text{tot}}}vN_{\text{r}}\,Y_{\text{r}}
\end{aligned} \qquad [4]$$

Here, v is the volume of a single cell, $V_{\text{m}} = V_{\text{tot}} - v\,(N_{\text{s}} + N_{\text{r}})$ is the volume of the medium, Y_0 is the concentration of Cm in the inflow medium, P measures the permeability of the cell membrane for Cm, and the function D quantifies the per-capita degradation rate of the antibiotic. We assume that the degradation of Cm by CAT follows Michaelis-Menten kinetics, i.e., $\text{D}(Y) = d_{\text{max}}\,Y\,/\,(K_{\text{Y}} + Y)$, where d_{max} is the maximum degradation rate and K_{Y} is the half-saturation constant of CAT for Cm.

The growth of the two bacterial populations is assumed to be proportional to their respective rates of resource consumption, but we consider that CAT expression may have a negative effect on the growth rate of Cm^R cells. This potential cost is incorporated by

allowing for different growth rate conversion factors g_s and g_r of the Cm^S and Cm^R cells. The population growth equations are thus given by:

$$\begin{aligned} \frac{dN_s}{dt} &= g_s C(Z, Y_s) N_s - \frac{Q}{V_{tot}} N_s \\ \frac{dN_r}{dt} &= g_r C(Z, Y_r) N_r - \frac{Q}{V_{tot}} N_r \end{aligned} \quad [5]$$

For simplicity, cell death is assumed to occur at a negligible rate, even in the presence of Cm, so cells are lost only through outflow from the chemostat. (This assumption can be relaxed, if necessary, by incorporating a positive rate of autolysis. The general analysis below, however, shows that this has no qualitative effect on the conclusions, as long as the net growth rate decreases monotonically with the intracellular concentration of antibiotic).

The bacteriostatic effect of the antibiotic is modeled as a non-competitive inhibition of the resource consumption rate, $C(Z, Y)$, which also depends on the resource concentration according to Michaelis-Menten kinetics. To be exact:

$$C(Z, Y) = c_{max} \frac{Z}{K_Z + Z} \frac{H_Y}{H_Y + Y} \quad [6]$$

where c_{max} is the maximum per-capita resource uptake rate in medium with a growth-saturating concentration of the resource and no antibiotic. All else being equal, cell growth is reduced by 50% relative to its value without antibiotic at Cm concentration $Y = H_Y$. Similarly, half-saturated growth occurs at resource concentration $Z = K_Z$.

S1.2. Rescaling. The model is next transformed into a dimensionless form, in order to reduce the number of free parameters. This rescaling step is accomplished by expressing the cell densities of Cm^S and Cm^R cells as volume fractions ($x_s = N_s\, v / V_{tot}$ and $x_r = N_r\, v / V_{tot}$), measuring time relative to the chemostat dilution time ($\tau = t\, Q / V_{tot}$) and scaling the resource and Cm concentrations relative to their respective concentrations in the inflow medium ($z_r = Z_r / Z_0$, $y_m = Y_m / Y_0$, $y_s = Y_s / Y_0$, $y_r = Y_r / Y_0$). The resulting equations for the growth of the two bacterial populations are given by:

$$\begin{aligned} \frac{dx_s}{d\tau} &= x_s \rho(z, y_s) - x_s \\ \frac{dx_r}{d\tau} &= \eta x_r \rho(z, y_r) - x_r \end{aligned} \quad [7]$$

where:

$$\rho(z, y) = r \frac{z}{k_z + z} \frac{h_y}{h_y + y} \quad [8]$$

is the scaled growth rate function, $r = g_s\, c_{max}\, V_{tot} / Q$ is the (scaled) maximum growth rate of the Cm^S cells, and $k_z = K_Z / Z_0$ and $h_y = H_y / Y_0$, respectively, are the (scaled) half-saturation and inhibitory constants of the growth function. The parameter $\eta = g_r / g_s$ quantifies how efficiently the Cm^R strain grows relative to the susceptible one, which is a measure for the fitness cost of CAT expression.

For the resource concentration, we obtain:

$$\frac{dz}{d\tau} = (1 - z) - c x_s \rho(z, y_s) - c x_r \rho(z, y_r) \qquad [9]$$

Here, $c = 1 / (g_s\, v\, Z_0)$ reflects the amount of resource needed to grow a volume unit of cells.

For the equations describing the Cm concentrations, we worked out the products in the derivatives on the left-hand side of equations [4]. The resulting equations:

$$\begin{aligned} \frac{dy_m}{d\tau} &= \left(\frac{1}{1-x_s-x_r} - y_m\right) - p\,\frac{x_s(y_m-y_s)+x_r(y_m-y_r)}{1-x_s-x_r} - y_m\,\frac{d\ln(1-x_s-x_r)}{d\tau} \\ \frac{dy_s}{d\tau} &= p(y_m - y_s) - y_s \rho(z, y_s) \\ \frac{dy_r}{d\tau} &= p(y_m - y_r) - \delta(y_r) - y_r \eta \rho(z, y_r) \end{aligned} \qquad [10]$$

have an additional term on the right-hand side that captures the effect of changes in medium volume and dilution of intracellular Cm due to cell growth. The rate of exchange between the compartments depends on the relative permeability $p = P\, V_{tot} / (v\, Q)$ of the cells to Cm. Finally, $\delta(y) = d\, y / (k_y + y)$, the rate of degradation of Cm by CAT, is characterized by two dimensionless parameters, a maximum rate $d = d_{max}\, V_{tot} / (v\, Y_0\, Q)$, and a half-saturation constant $k_y = K_Y / Y_0$.

S1.3. Qualitative model analysis. In order to characterize the conditions that allow for stable coexistence between the two strains (e.g. Fig. 3), we next perform a qualitative equilibrium stability analysis of the model (equations [7] to [10]). Accordingly, we suppose that the Cm^S and Cm^R cells attain equilibrium densities of x_s^* and x_r^*, respectively, and then ask under what conditions this equilibrium exists and is stable.

At equilibrium, the two net population growth rates must be zero, so that we obtain a first equilibrium condition from equation [7]:

$$\rho(z^*, y_s^*) = \eta \rho(z^*, y_r^*) = 1 \qquad [11]$$

This condition states that the loss of cells from the chemostat must be balanced by cell growth for both cell types. Here (and throughout), equilibrium values of variables are

marked with an asterisk. Based on equality 11], the equilibrium conditions for the intracellular concentrations of Cm (equations [10]; $dy_S/d\tau = 0$ and $dy_r/d\tau = 0$) lead to the obvious result that:

$$y_r^* = \frac{py_m^* - \delta(y_r^*)}{p+1} < \frac{py_m^*}{p+1} = y_S^* \quad \text{for any } y_r^* > 0 \qquad [12]$$

i.e., the intracellular concentration of Cm in Cm^R cells is lower than in Cm^S cells, given that $\delta(y_r^*) > 0$ for any $y_r^* > 0$.

Given that Cm inhibits cell growth ($\rho(z, y)$ is a monotonically decreasing function of y, condition [12] implies that $\rho(z^*, y_S^*) < \rho(z^*, y_r^*)$. Hence, condition [11] can only be satisfied if:

$$\eta = \frac{\rho(z^*, y_S^*)}{\rho(z^*, y_r^*)} < 1 \qquad [13]$$

From this general result, we conclude that coexistence between Cm^S and Cm^R strains can be achieved only when CAT expression is costly.

In order to assess the stability of the coexistence equilibrium, we must take into consideration the ecological feedback between the bacterial populations and their environment, specifically, the concentration of Cm in the medium. If this environmental feedback is weak, y_S^* and y_r^* will vary only little with the relative frequencies of the two strains, implying that condition [11] can be satisfied for only a limited range of values for η. Conversely, robust coexistence relies on a strong environmental feedback, in which the Cm^R cells must exert a high level of control over the extracellular concentration of chloramphenicol. This requires that the strain must be able to reach a high population density. In a well-mixed chemostat model, coexistence is therefore observed only when the cell volume fractions reach high values (>20%); however, in spatially structured environments, cells can have a large influence on their local environment even if the overall population size is small.

S1.4. Numerical bifurcation analysis. While a strong environmental feedback is necessary for robust coexistence, such coexistence must also be dynamically stable. To evaluate the stability of coexistence between Cm^S and Cm^R strains, we performed extensive numerical simulations across a range of parameter conditions and classified the dynamics of the model based on the number and the stability of the equilibria that were observed in these

simulations (S3 Fig.). One general observation across the whole set of simulations is that if interior equilibria ($x_S^* > 0$ and $x_r^* > 0$) are present, always at least one of them is stable. In particular, there was no parameter condition for which we found mutual exclusion, i.e., an unstable interior equilibrium from which small departures lead to a population dominated by either one or the other cell type depending on the initial abundances.

These results are explained by the fact that the marginal impact of Cm^R cells on the chemostat environment diminishes as the Cm^R strain becomes more abundant. Figure 3b shows clearly why this is the case: the invasion of Cm^R cells causes a reduction in the intra- (and extra-)cellular Cm concentrations, strongly decreasing the level of antibiotic stress for both types of cells. At lower stress levels, the relative advantage of Cm degradation is lower as well. As the Cm^R population continues to grow, the relative growth rate bonus of Cm^R cells may eventually become so low that it is exactly balanced by the cost of CAT expression. When that happens, stable coexistence between Cm^R and Cm^S strains can be maintained dynamically, satisfying equilibrium condition [11].

The frequency-dependent effect of Cm^R cells on the environment also explains why we observe bistability in a large region of the parameter space (areas between dashed and solid blue lines in S3 Fig.). In this area, a population of Cm^R cells can maintain itself at high density, but cannot invade an empty chemostat inoculated with a few individuals. Here, a large population of Cm^R cells is necessary to reduce the Cm concentration below the critical concentration that still permits persistent growth in the chemostat.

Given that the Cm^S strain is a superior competitor, it is possible for that strain to push the Cm^R cells below their critical density. When this happens, and the Cm^S strain cannot survive on its own, we observe competition-induced extinction (S4 Fig.). In this regime, a population of Cm^R cells is first invaded by the susceptible strain and eventually outcompeted. The remaining Cm^S cells, however, cannot survive on their own, as the concentration of antibiotic is no longer kept low by the resistant cells. This counter-intuitive process is an example of the 'resident-strikes-back' phenomenon (Mylius & Diekmann, 2001), which has received previous attention in the theoretical literature.

S1 Text Reference. Mylius, S. D., Diekmann, O. The resident strikes back: invader-induced switching of resident attractor. *J. Theor. Biol.* 211: 297-311 (2001).

Supplementary Figures

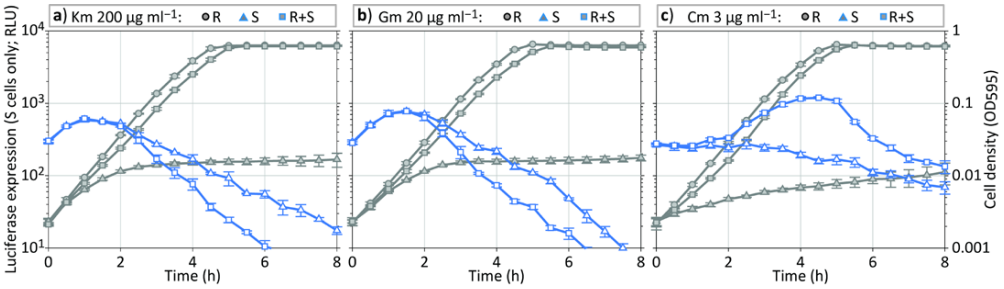

S1 Figure | Antibiotic degradation in the pneumococcus. (**a–c**) Plate reader assay sets in quadruplicate (average and s.e.m.) measuring luciferase expression (symbols with color outline) and cell density (corresponding grey symbols) of resistant (R), susceptible (S) and a mixture of resistant and susceptible (R+S) *S. pneumoniae* cells growing in the presence of 200 µg ml^{-1} kanamycin (**a**), 20 µg ml^{-1} gentamycin (**b**), and 3 µg ml^{-1} chloramphenicol (**c**). Assays with resistant cells (R) were inoculated to a density of OD 0.002, mixed populations (R+S) to a density of OD 0.001 each, and susceptible cells-only (S) also to a density of OD 0.001 with the addition of equal amounts of D39 wild type cells to correct for unspecific effects such as cellular drug binding. D-PEP22 that constitutively expresses firefly luciferase was used throughout as susceptible strain. Resistant strains expressed *aphA1* (**a**), *aacCI* (**b**), and *cat* (**c**). Note that in aminoglycoside-inhibited cultures (**a** and **b**) luminescence of R+S assays decreased more rapidly compared with S assays. This can be explained by reduced luciferase expression rates when cultures exceed OD 0.05; S cultures, in contrast to R+S cultures, do not reach OD 0.05 and consequently continue to express luciferase at a higher rate.

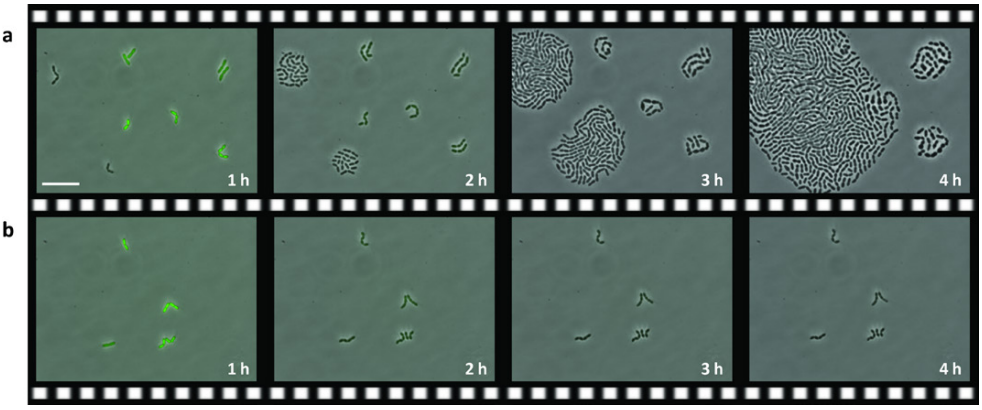

S2 Figure | Single-cell analysis of pneumococcal collective resistance. (**a**, **b**) Still images (overlay of phase contrast and fluorescence microscopy) of a time-lapse experiment of chloramphenicol-susceptible *S. pneumoniae* D-PEP33 cells that constitutively express GFP, either co-cultivated with the CAT-expressing *S. pneumoniae* D-PEP1-pJS5 (**a**) or in

monoculture (**b**), growing on a semi-solid surface supplemented with 3 µg ml^{-1} chloramphenicol. High inoculation densities were spotted, resulting in rapid chloramphenicol deactivation in the co-cultivation assay. Note that GFP, which allows for the distinction between chloramphenicol-susceptible and -resistant cells at the beginning of the time-lapse experiment (fluorescent versus non-fluorescent), bleaches quickly in the course of the assay; inhibited susceptible cells, even after (partial) Cm clearance, do not express sufficient levels of GFP (counteracting photobleaching) to allow for a continuous detection. Scale bar, 10 µm.

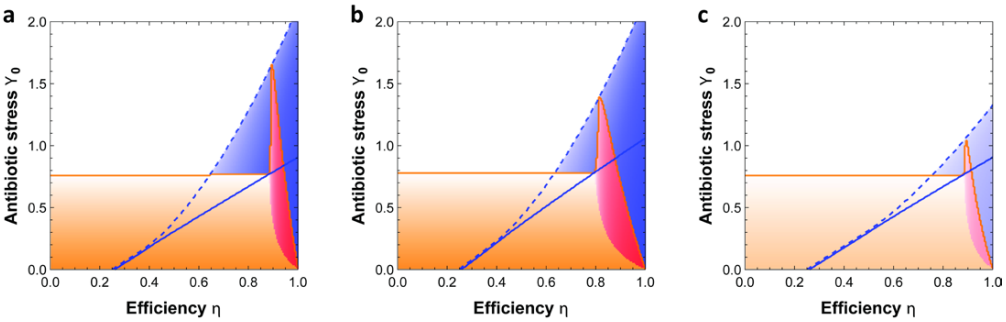

S3 Figure | Numerical model analysis. (**a**–**c**) Colored areas indicate qualitatively different outcomes of competition between Cm^S and Cm^R cells in model simulations, as a function of two key parameters: the growth rate efficiency of Cm^R cells ($1 - \eta$ quantifies the cost of CAT expression), and the concentration of Cm in the inflow medium (Y_0; antibiotic stress). (**a**) An orange line borders the region in which the Cm^S strain can grow from low initial density. This is below a critical level of antibiotic stress, or in a narrow range of η values when the resistant cells are present. The Cm^R strain can grow from low initial density in the area bordered by a solid blue line, but can maintain high population densities over a larger area of parameter space (i.e., in the area bordered by a dashed blue line). Stable coexistence of both strains is maintained in a narrow parameter region (red area). When η is close to 1, Cm^R is always a superior competitor (dark blue area), in line with the analytical result that coexistence cannot be maintained unless CAT expression is costly. When CAT expression costs are high, Cm^S tends to outcompete Cm^R. However, this process leads to an elevation of Cm in the medium, which may eventually cause both strains to go extinct (light blue area; here, Cm^R can survive on its own, but not when Cm^S is also present; see S4 Fig.). Alternatively, Cm^S can persist on its own after driving Cm^R to extinction (orange area). Parameters are: $r = 20.0$, $k_z = 4.0$, $c = 1.0$, $p = 50.0$, $h_Y = 0.25/Y_0$, $k_Y = 2.5/Y_0$ and $d = 30.0/Y_0$. In (**b**) the relative benefit of CAT degradation is larger, due to a slower diffusion of Cm across the cell membrane ($p = 25.0$; other parameters as in **a**). (**c**) This panel illustrates the effect of a change in the resource consumption rate c which affects the equilibrium population densities ($c = 2.0$; other parameters as in **a**). In this case, Cm^R and Cm^S reach lower equilibrium densities, weakening the effect of Cm^R on the environment. As a result, the conditions for coexistence become more stringent. Throughout, we performed multiple simulations per parameter condition to search for boundary and interior equilibria, and classified the dynamics based on the stability properties of the equilibria. Color saturation within each area gives an indication of the total cell density at equilibrium.

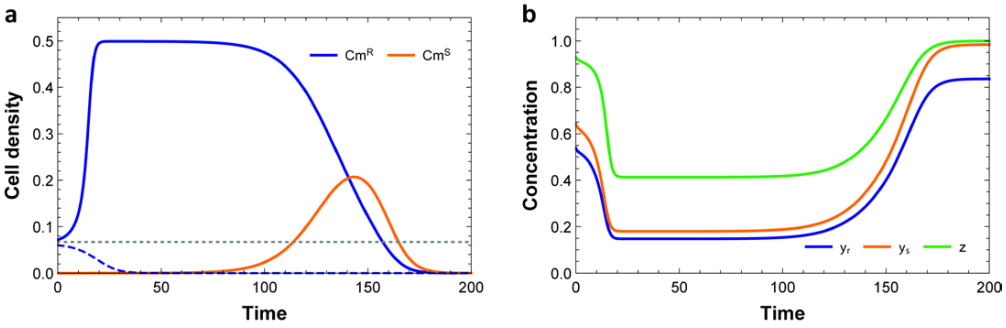

S4 Figure | Extinction induced by competition. (**a**) Simulated growth trajectories for Cm^R and Cm^S populations subject to antibiotic stress and competition for a limiting resource. Here, the Cm^R strain is an inferior competitor that is driven to extinction by the invasion of Cm^S cells, even though the growth conditions are not permissive for the survival of Cm^S on its own. Extinction is caused by a bistability in the growth dynamic of Cm^R cells: a critical cell density is required to lower the concentration of Cm below the level that permits population growth. The initial Cm^R cell density in the simulation was just above this critical level (indicated by a dotted gray line); the Cm^R cells are not able to invade if their initial density lies below the threshold (shown by the dashed blue trajectory). However, after successful invasion (solid blue trajectory), the Cm^R cells can still be pushed below their critical density by competition with the Cm^S strain, triggering the collapse of both populations. (**b**) Dynamics of intracellular Cm concentrations and resource. Parameters are: $r = 20.0$, $\eta = 0.85$, $k_z = 4.0$, $c = 1.0$, $p = 50.0$, $h_Y = 0.25$, $k_Y = 2.5$ and $d = 30.0$.

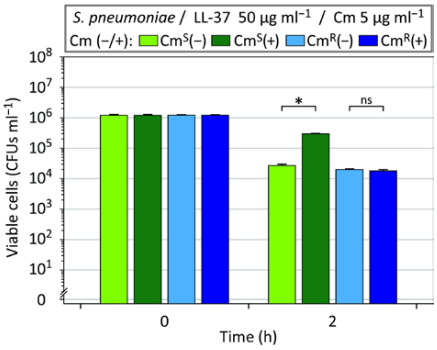

S5 Figure | LL-37 activity in dependency on chloramphenicol. Killing of Cm-susceptible *S. pneumoniae* D-PEP2K1 (Cm^S) and Cm-resistant D-PEP1C3 (Cm^R) by the human antimicrobial peptide LL-37 at a concentration of 50 µg ml^{-1}, in absence (−) or presence (+) of 5 µg ml^{-1} chloramphenicol (Cm); average and s.e.m. of duplicates are shown. *P < 0.05; two-tailed t-test.

Acknowledgements

We thank M. Espinosa for plasmid pJS5, R. Nijland for *S. aureus* strain LAC pCM29, M. Montalban and M. Bartholomae for assistance with the HPLC system and Lingjun He for support with statistical analysis.

Author Contributions

R.A.S and J.W.V. initiated the project. R.A.S. and M.S. performed *in vitro* experiments. L.L. and J.O. performed *in vivo* mouse experiments. G.S.v.D. performed mathematical modeling. R.A.S., L.L., G.S.v.D., V.N., and J.W.V. designed the experiments and wrote the manuscript.

References

1. World Health Organization. Antimicrobial resistance: global report on surveillance 2014. http://www.who.int/drugresistance/documents/surveillancereport/en.
2. Vega, N. M. & Gore, J. Collective antibiotic resistance: mechanisms and implications. *Curr. Opin. Microbiol.* 21C, 28–34 (2014).
3. Levin, B. R. & Rozen, D. E. Non-inherited antibiotic resistance. *Nat. Rev. Microbiol.* 4, 556–562 (2006).
4. Chi, D. H. et al. Nasopharyngeal reservoir of bacterial otitis media and sinusitis pathogens in adults during wellness and viral respiratory illness. *Am. J. Rhinol.* 17, 209–214 (2003).
5. Allen, E. K. et al. Characterization of the nasopharyngeal microbiota in health and during rhinovirus challenge. *Microbiome* 2, 22 (2014).
6. Teo, S. M. et al. The infant nasopharyngeal microbiome impacts severity of lower respiratory infection and risk of asthma development. *Cell Host Microbe* 17, 704–715 (2015).
7. Kirby, A. E., Garner, K. & Levin, B. R. The relative contributions of physical structure and cell density to the antibiotic susceptibility of bacteria in biofilms. *Antimicrob. Agents Chemother.* 56, 2967–2975 (2012).
8. Lebeaux, D., Ghigo, J.-M. & Beloin, C. Biofilm-related infections: bridging the gap between clinical management and fundamental aspects of recalcitrance toward antibiotics. *Microbiol. Mol. Biol. Rev. MMBR* 78, 510–543 (2014).
9. Ackermann, M. A functional perspective on phenotypic heterogeneity in microorganisms. *Nat. Rev. Microbiol.* 13, 497–508 (2015).

10. Tuomanen, E., Cozens, R., Tosch, W., Zak, O. & Tomasz, A. The rate of killing of *Escherichia coli* by beta-lactam antibiotics is strictly proportional to the rate of bacterial growth. *J. Gen. Microbiol.* 132, 1297–1304 (1986).
11. Eng, R. H., Padberg, F. T., Smith, S. M., Tan, E. N. & Cherubin, C. E. Bactericidal effects of antibiotics on slowly growing and nongrowing bacteria. *Antimicrob. Agents Chemother.* 35, 1824–1828 (1991).
12. Sorg, R. A. & Veening, J.-W. Microscale insights into pneumococcal antibiotic mutant selection windows. *Nat. Commun.* 6, 8773 (2015).
13. Balaban, N. Q., Merrin, J., Chait, R., Kowalik, L. & Leibler, S. Bacterial persistence as a phenotypic switch. *Science* 305, 1622–1625 (2004).
14. Gerdes, K. & Maisonneuve, E. Bacterial persistence and toxin-antitoxin loci. *Annu. Rev. Microbiol.* 66, 103–123 (2012).
15. Prudhomme, M., Attaiech, L., Sanchez, G., Martin, B. & Claverys, J.-P. Antibiotic stress induces genetic transformability in the human pathogen *Streptococcus pneumoniae*. *Science* 313, 89–92 (2006).
16. Stevens, K. E., Chang, D., Zwack, E. E. & Sebert, M. E. Competence in *Streptococcus pneumoniae* is regulated by the rate of ribosomal decoding errors. *mBio* 2, (2011).
17. Slager, J., Kjos, M., Attaiech, L. & Veening, J.-W. Antibiotic-induced replication stress triggers bacterial competence by increasing gene dosage near the origin. *Cell* 157, 395–406 (2014).
18. Lee, H. H., Molla, M. N., Cantor, C. R. & Collins, J. J. Bacterial charity work leads to population-wide resistance. *Nature* 467, 82–85 (2010).
19. Brook, I. Inoculum effect. *Rev. Infect. Dis.* 11, 361–368 (1989).
20. Dugatkin, L. A., Perlin, M., Lucas, J. S. & Atlas, R. Group-beneficial traits, frequency-dependent selection and genotypic diversity: an antibiotic resistance paradigm. *Proc. Biol. Sci.* 272, 79–83 (2005).
21. Yurtsev, E. A., Chao, H. X., Datta, M. S., Artemova, T. & Gore, J. Bacterial cheating drives the population dynamics of cooperative antibiotic resistance plasmids. *Mol. Syst. Biol.* 9, 683 (2013).
22. Medaney, F., Dimitriu, T., Ellis, R. J. & Raymond, B. Live to cheat another day: bacterial dormancy facilitates the social exploitation of β-lactamases. *ISME J.* 10, 778–787 (2016).
23. Brook, I. The role of beta-lactamase-producing bacteria in the persistence of streptococcal tonsillar infection. *Rev. Infect. Dis.* 6, 601–607 (1984).
24. Weimer, K. E. D. et al. Divergent mechanisms for passive pneumococcal resistance to β-lactam antibiotics in the presence of *Haemophilus influenzae*. *J. Infect. Dis.* 203, 549–555 (2011).

25. Brook, I. The role of beta-lactamase-producing-bacteria in mixed infections. *BMC Infect. Dis.* 9, 202 (2009).

26. Shaw, W. V. The enzymatic acetylation of chloramphenicol by extracts of R factor-resistant *Escherichia coli*. *J. Biol. Chem.* 242, 687–693 (1967).

27. Suzuki, Y. & Okamoto, S. The enzymatic acetylation of chloramphenicol by the multiple drug-resistant *Escherichia coli* carrying R factor. *J. Biol. Chem.* 242, 4722–4730 (1967).

28. Shaw, W. V. & Unowsky, J. Mechanism of R factor-mediated chloramphenicol resistance. *J. Bacteriol.* 95, 1976–1978 (1968).

29. Nicoloff, H. & Andersson, D. I. Indirect resistance to several classes of antibiotics in cocultures with resistant bacteria expressing antibiotic-modifying or -degrading enzymes. *J. Antimicrob. Chemother.* 71, 100–110 (2016).

30. Yurtsev, E. A., Conwill, A. & Gore, J. Oscillatory dynamics in a bacterial cross-protection mutualism. *Proc. Natl. Acad. Sci. U. S. A.* 113, 6236–6241 (2016).

31. Tomasz, A. Antibiotic resistance in *Streptococcus pneumoniae*. *Clin. Infect. Dis.* 24, S85–S88 (1997).

32. Lewis, K. Platforms for antibiotic discovery. *Nat. Rev. Drug Discov.* 12, 371–387 (2013).

33. Chewapreecha, C. et al. Dense genomic sampling identifies highways of pneumococcal recombination. *Nat. Genet.* 46, 305–309 (2014).

34. World Health Organization. Model list of essential medicines 2015. http://www.who.int/selection_medicines/committees/expert/20/EML_2015_FINAL_amended_AUG2015.pdf?ua=1.

35. Falagas, M. E., Grammatikos, A. P. & Michalopoulos, A. Potential of old-generation antibiotics to address current need for new antibiotics. *Expert Rev. Anti Infect. Ther.* 6, 593–600 (2008).

36. Maviglia, R., Nestorini, R. & Pennisi, M. Role of old antibiotics in multidrug resistant bacterial infections. *Curr. Drug Targets* 10, 895–905 (2009).

37. Nitzan, O. et al. Is chloramphenicol making a comeback? *Isr. Med. Assoc. J. IMAJ* 12, 371–374 (2010).

38. Avery, O. T., Macleod, C. M. & McCarty, M. Studies on the chemical nature of the substance inducing transformation of pneumococcal types : induction of transformation by a desoxyribonucleic acid fraction isolated from pneumococcus type III. *J. Exp. Med.* 79, 137–158 (1944).

39. Robins-Brown, R. M. et al. Resistance mechanisms of multiply resistant pneumococci: antibiotic degradation studies. *Antimicrob. Agents Chemother.* 15, 470–474 (1979).

40. Taber, H. W., Mueller, J. P., Miller, P. F. & Arrow, A. S. Bacterial uptake of aminoglycoside antibiotics. *Microbiol. Rev.* 51, 439–457 (1987).

41. Sorg, R. A., Kuipers, O. P. & Veening, J.-W. Gene expression platform for synthetic biology in the human pathogen *Streptococcus pneumoniae*. *ACS Synth. Biol.* 4, 228–239 (2015).

42. Ballester, S., Lopez, P., Alonso, J. C., Espinosa, M. & Lacks, S. A. Selective advantage of deletions enhancing chloramphenicol acetyltransferase gene expression in *Streptococcus pneumoniae* plasmids. *Gene* 41, 153–163 (1986).

43. Feder, H. M. Chloramphenicol: what we have learned in the last decade. *South. Med. J.* 79, 1129–1134 (1986).

44. Branca, C. et al. Non-radioactive detection of β-glucuronidase and chloramphenicol acetyltransferase activities in co-transformed protoplasts by HPLC. *Plant Cell Rep.* 12, 361–365 (1993).

45. Hardin, G. The competitive exclusion principle. *Science* 131, 1292–1297 (1960).

46. Kristian, S. A. et al. Impairment of innate immune killing mechanisms by bacteriostatic antibiotics. *FASEB J. Off. Publ. Fed. Am. Soc. Exp. Biol.* 21, 1107–1116 (2007).

47. Hu, Y. et al. Metagenome-wide analysis of antibiotic resistance genes in a large cohort of human gut microbiota. *Nat. Commun.* 4, 2151 (2013).

48. van Schaik, W. The human gut resistome. *Philos. Trans. R. Soc. Lond. B. Biol. Sci.* 370, 20140087 (2015).

49. Moore, A. M. et al. Gut resistome development in healthy twin pairs in the first year of life. *Microbiome* 3, 27 (2015).

50. Van Boeckel, T. P. et al. Global antibiotic consumption 2000 to 2010: an analysis of national pharmaceutical sales data. *Lancet Infect. Dis.* 14, 742–750 (2014).

51. Robicsek, A. et al. Fluoroquinolone-modifying enzyme: a new adaptation of a common aminoglycoside acetyltransferase. *Nat. Med.* 12, 83–88 (2006).

52. Halfmann, A., Hakenbeck, R. & Brückner, R. A new integrative reporter plasmid for *Streptococcus pneumoniae*. *FEMS Microbiol. Lett.* 268, 217–224 (2007).

53. Prudhomme M, Claverys J-P. There will be a light: the use of *luc* transcriptional fusions in living pneumococcal cells. In "The Molecular Biology of Streptococci." Horizon Scientific Press; 2007. pp. 519-524

54. Pang, Y. Y. et al. agr-Dependent interactions of *Staphylococcus aureus* USA300 with human polymorphonuclear neutrophils. *J. Innate Immun.* 2, 546–559 (2010).

55. Bergé, M., Moscoso, M., Prudhomme, M., Martin, B. & Claverys, J.-P. Uptake of transforming DNA in Gram-positive bacteria: a view from *Streptococcus pneumoniae*. *Mol. Microbiol.* 45, 411–421 (2002).

56. Revelli, D. A., Boylan, J. A. & Gherardini, F. C. A non-invasive intratracheal inoculation method for the study of pulmonary melioidosis. *Front. Cell. Infect. Microbiol.* 2, 164 (2012).